JMEPEG (2022) 31:8148–8159
https://doi.org/10.1007/s11665-022-06875-5

©ASM International
1059-9495/$19.00

TECHNICAL ARTICLE

# Fabrication and Experimental Study of Micro-gripper with Electrothermal Actuation by Stereolithography Method

*Osman Ulkir, Ishak Ertugrul, Nihat Akkus, and Salih Ozer*

Submitted: 19 August 2021 / Revised: 14 January 2022 / Accepted: 4 March 2022 / Published online: 18 April 2022

**The aim of the study is to get high displacement values with low actuation voltage from the micro-gripper fabricated by stereolithography (SLA) method. Micro-grippers are devices based on a micro-electro-mechanical system (MEMS) preferred for manipulation and assembly in micro-fabrication. This article presents the modeling, fabrication, and experimental studies of a U-type electrothermal MEMS micro-gripper. The fabrication of the gripper was made by SLA, which is one of the additive manufacturing methods. The arm tip displacement of the gripper has been characterized in real-time by optical microscopy. In electrical characterization studies, the electrical voltage was applied to the pads of the micro-gripper. This voltage value was increased starting from 0V with 1V increments until deterioration was observed in the gripper. The micro-gripper is shown to actuate to a maximum opening displacement of 28.35 $\mu$m at an applied voltage of 5V. The models are employed to examine key factors of the micro-gripper's performance including temperature distribution, displacement, and stresses based on an elastic analysis of structures. Experimental results for the displacement of the micro-gripper's arm tips were found to be in good agreement with the simulation results.**

**Keywords** additive manufacturing, electrothermal actuation, electrical characterization, MEMS, stereolithography, tip displacement

## 1. Introduction

Micro-electro-mechanical system (MEMS) is a process technology comprising miniaturized mechanical and electro-mechanical parts made using micro-fabrication methods (Ref 1-3). In recent years, MEMS technology has led to the development of various new technologies in the fields of science and engineering. Micro-grippers are on MEMS devices that are usually used in the fields of micro-assembly and micromanipulation. They play critical roles in the handling and position control of micro-mechanical objects such as micro-mechanical parts and biological cells. Micro-grippers have been the subject of many studies in terms of micro-gripper design, mechanical structure, detection principle, operational aspects, microfabrication, and applicability to different environments (Ref 4-7).

An actuation mechanism is an important component in all active MEMS devices because it provides the device's necessary motions. MEMS-based micro-grippers can be classified into six groups according to the actuation mechanism: piezoelectric, electrostatic, electrothermal, pneumatic, electromagnetic, and shape memory alloy (Ref 8-10). Electrostatic actuation required a high operating voltage (Ref 11). This voltage value typically is between 10 and 200V to operate (Ref 12). Shape memory alloys (SMA) have low grip strength (Ref 13). Designed using SMA micro-actuator is 5.14 mm in diameter and 40 mm and is used to actuate 20-mm-long needle driver assembly, while generating a force of 24 N, resulting in a gripping force of 8 N (Ref 14). Piezoelectric structures can generate a high grip force but at much lower stroke (Ref 15). For example, a micro-gripper can produce a gripping force of 300 mg in piezoelectric operation while having a maximum stroke of 110 $\mu$m out-of-plane and 30 $\mu$m in-plane no-load at $\pm$ 100 V DC (Ref 16). Drawbacks, such as high power consumption and a difficult fabrication method for depositing ferromagnetic materials on a micro-actuator constrain electromagnetic implementation (Ref 17). The experimental results in one study showed that an electromagnetically actuated micro-gripper performed excellently in terms of large tip displacement (165 $\mu$m) and good holding force (15 $\mu$N) under relatively low voltage (3V) with a power consumption of 5 W (Ref 18). Since pneumatic mechanisms use air as an energy source, it makes it difficult to control the micro-system (Ref 19). The electrothermal actuation mechanism has been one of the first developed working principles within the MEMS field, mostly because of the benefits of a basic structure that can be made using proven technology with a few production steps (Ref 20). The operating principle of electrothermal mechanisms depends on the differential thermal expansion of well-designed structures caused by resistive heating to work. These mechanisms often have a range of advantages over other actuation systems, such as the ability

**Osman Ulkir**, Department of Electronics and Automation, Mus Alparslan University, 49210 Mus, Turkey; **Ishak Ertugrul**, Department of Mechatronics, Mus Alparslan University, 49210 Mus, Turkey; **Nihat Akkus**, Department of Mechatronics Engineering, Gedik University, 34210 Istanbul, Turkey; and **Salih Ozer**, Department of Mechanical Engineering, Mus Alparslan University, 49210 Mus, Turkey. Contact e-mail: o.ulkir@alparslan.edu.tr.

to produce a significant output power and displacement with a low voltage. Thus, high gripping force can be got from the micro-gripper (Ref 21). Because of such advantages, we employed the electrothermal operation to the micro-gripper in this study.

In recent years, many studies have been conducted in the literature on the design, mechanical structure, manufacturing method, and applicability of MEMS micro-grippers to different environments (Ref 22-28). Previous works on MEMS micro-grippers have focused on the optimization of their design and kinematic structure (Ref 29), the structural materials used (Ref 30), the actuation and sensing mechanisms, the operational requirements and limitations (Ref 31), the fabrication process used (Ref 32), and the working environment in which they will be operated (Ref 33). The most important aim in these studies is to obtain high displacement values with low actuation voltage. Until today, traditional micro-fabrication techniques such as lithography and photolithography have been preferred in the fabrication of MEMS-based micro-grippers (Ref 34, 35). Although these techniques have high precision and accuracy, they have disadvantages due to many process steps, long-term fabrication, and the need for a clean room. Nowadays, additive manufacturing technology takes the place of these fabrication techniques. This fabrication technique is accomplished by modeling from your desktop computer and using 3D printers, without requiring a lot of manufacturing processes and clean rooms. Although MEMS applications such as biomedical (Ref 36) and robotics (Ref 37) have been fabricated with this manufacturing technique, the micro-gripper device has not been fabricated before. With this study, an electrothermal MEMS micro-gripper was fabricated for the first time using stereolithography, one of the 3D printing methods.

Today, 3D fabrication technology uses printing methods such as stereolithography (SLA), digital light process (DLP), selective laser sintering (SLS), fused deposition modeling (FDM), and electron beam melting (EBM) (Ref 38-44). In this study, SLA method was preferred in the fabrication of micro-gripper. With this method, it is possible to create many complex structures with high resolution. In the SLA technology, a scanning laser is used to selectively polymerize a liquid polymer resin layer by layer for fabrication (Ref 45, 46). The SLA manufacturing process has been used to fabricate many microstructures and nanostructures for a wide variety of applications such as micro-sensors, micro-robotics, and microfluidic devices (Ref 47-49).

This article presents the fabrication, simulation modeling, and characterization experiments of a U-type electrothermal MEMS micro-gripper. Compared to existing micro-gripper designs (Ref 50-54), the proposed gripper structure provides a greater displacement with a lower voltage. The fabrication of the micro-gripper was carried out using the SLA method. They conducted an experimental study to examine the displacement of the fabricated gripper. Finite element analysis (FEA) was used to design, simulate and explore the properties of the micro-gripper. For validation, the simulation and experimental results of the micro-gripper are compared, and we showed the utility of the model as a design tool for specifying the displacement. In simulation and electrical characterization studies, the electrical voltage applied to displace the micro-gripper. This voltage value is determined by increasing from 0V with 1V increments until a deterioration in the gripper's structure is observed.

We arranged this study: Section 2 describes the design process, working principle, fabrication method of the micro-gripper, and simulation model of the micro-gripper. Section 3 describes the 3D fabrication process used to fabricate the micro-gripper and the experimental setup used for electrical characterization studies of the micro-gripper fabricated. Section 4 presents and compares numerical and experimental results for thermal and structural analysis of the micro-gripper. Finally, Sect. 5 shows the general result of the studies.

## 2. Materials and Methods

### 2.1 Micro-Gripper Design and Working Principle

The micro-gripper designed in this study is based on the micro-actuator design consisting of a "hot and cold arm" structure and the principle of electrothermal operation. The micro-actuator is a typical MEMS device used to design and control many micro devices made in the literature. This actuator consists of two arms of different sizes joined at their free ends to form a U-shaped electrical loop. These arms are limited by two anchors. The flexure arm is located between the cold arm and its anchor. The type of a U-type micro-actuator is shown in Fig. 1(a). The movement of this actuator is realized by differential thermal expansion between the arms.

The developed micro-gripper consists of two anti-symmetric U-type micro-actuators, two micro-gripper arms, and a gripper section to catch objects. 2D image and working principle of the micro-gripper are shown in Fig. 1(b). The action mechanism of the micro-gripper is realized as electrothermal actuation. This actuation is caused by the thermal expansion of different sizes of hot and cold arms. When voltage is applied to the gripper, with the current flow passing through the arms, the narrow arm (hot arm) heats more than the wider arm (cold arm) and experiences thermal expansion. This expansion causes a lateral (y-axis) displacement of the tip of the gripper in the direction of the cold arm. The temperature difference between the hot and cold arms affects the displacement of the micro-gripper.

As shown in Fig. 1(b), different from other studies in the literature, the micro-gripper is designed with three pad connectors, an arm tip, and a single photoconductor layer. In order for the micro-gripper to move in the lateral (y-axis) direction, the voltage must be given to the pads correctly. The same and positive voltage value is connected to 'PAD-1′ and 'PAD-3′. Surfaces and 'PAD-2′ ground connection is made. With these connections, lateral displacement is achieved when micro-gripper 'V' voltage is applied. The amount of displacement of the tip of the micro-gripper will vary depending on the applied voltage value.

The dimensioning and geometric structure of the micro-gripper, designed as a 3D using the computer-aided design (CAD) software, is shown in Fig. 2. Geometrical parameters (hot, cold, and flexure arm length, thickness, and width) and material properties (electrical and thermal conductivity parameters) affect the displacement performance of the micro-gripper. In this study, all geometric parameters were determined at the optimum level during 3D design. Material properties such as thermal and electrical conductivities were determined as fixed parameters in the COMSOL program during finite element analysis. The most important parameter in the displacement of the micro-gripper is the flexure arm. If this arm is long enough,

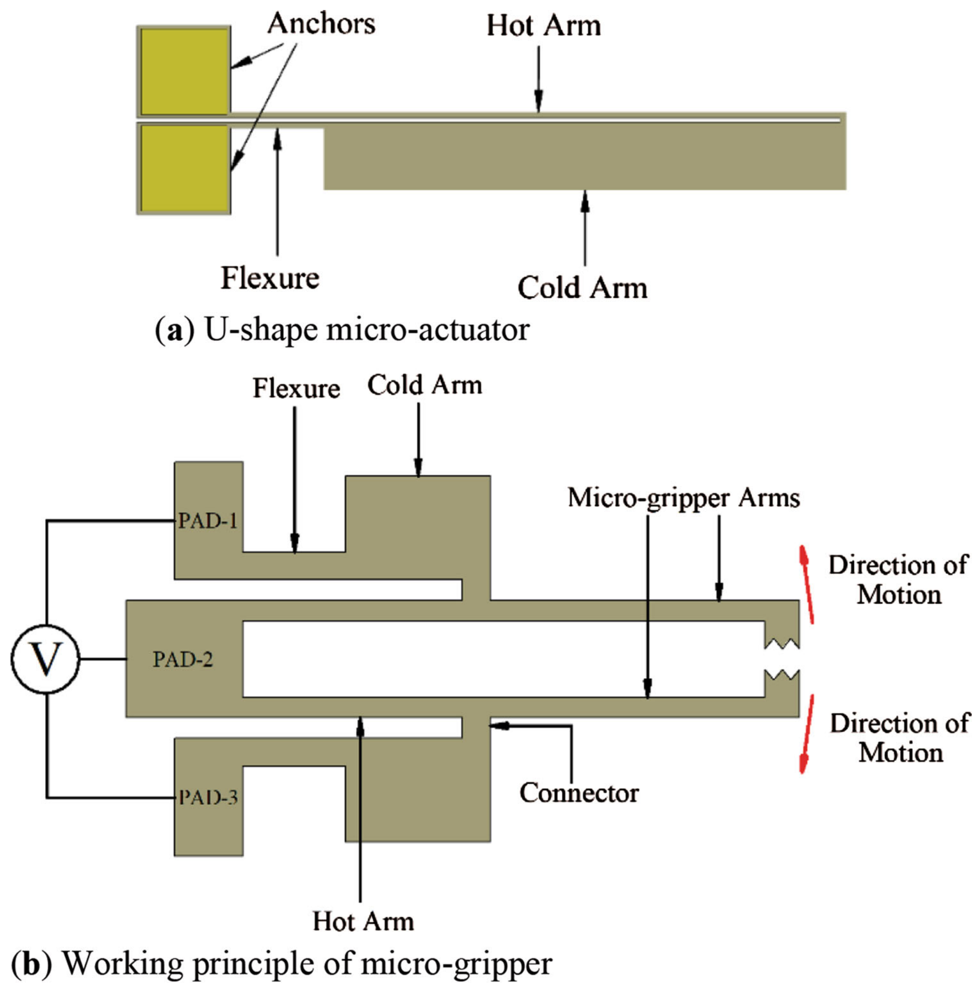


**Fig. 1** Electrothermal operating micro-actuator and micro-gripper structures

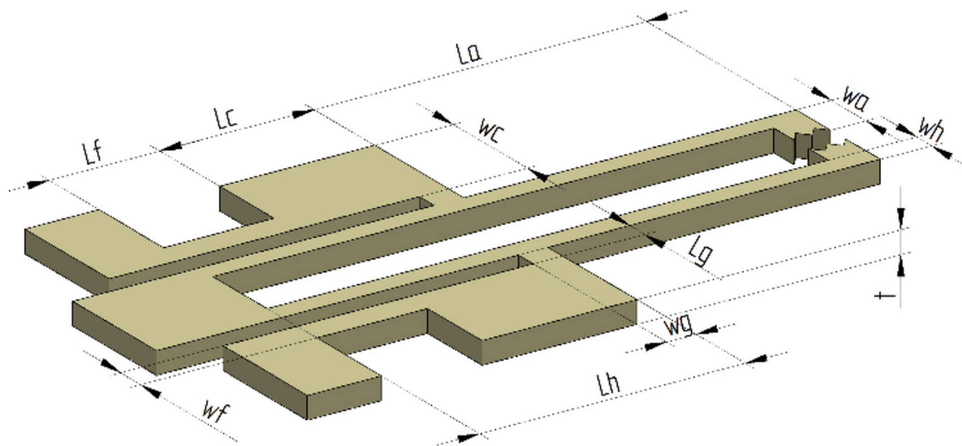


**Fig. 2** 3D CAD design and dimensions of the micro-gripper

it will increase the motion of the micro-gripper. The flexure arm is usually produced in the same width as the hot arm. However, the thinness of this arm can cause deformation by overheating. For this reason, the flexure arm should be wider than the hot arm.

The geometrical parameters of the designed micro-gripper are shown in Table 1. These values were got by considering the design criteria of the micro-gripper. The design in Fig. 2 was used in the fabrication process carried out with the stereo lithography method using a 3D printer. We used photoconductive resin for the fabrication of the micro-gripper designed from a single layer. We frequently used these materials in additive manufacturing technology because of their electrical properties.

**Table 1 Geometrical parameters of the micro-gripper**

| Parameter | Symbol | Value ($\mu$m) |
|---|---|---|
| Length of hot arm | $L_h$ | 500 |
| Length of cold arm | $L_c$ | 350 |
| Length of flexure arm | $L_f$ | 200 |
| Length of gripping arm | $L_a$ | 500 |
| Length of connector | $L_g$ | 70 |
| Width of hot arm | $w_h$ | 30 |
| Width of cold arm | $w_c$ | 100 |
| Width of flexure arm | $w_f$ | 35 |
| Width of gripping arm | $w_a$ | 45 |
| Width of connector | $w_g$ | 35 |
| Thickness of micro-gripper | $t$ | 5 |

### 2.2 Analytical Model

In this section, analytical modeling of the electrothermal micro-gripper is done. Resistive heating under an applied voltage produces the temperature of the micro-gripper's different actuator components to rise. The improved temperature distributions along the hot arm, $T_h(x)$, cold arm $T_c(x)$, and flexure $T_f(x)$ components are given by Eq. 1, 2 and 3, respectively [30].

$$T_h(x) = T_H + C_1 e^{m_h x} + C_2 e^{-m_h x} \quad \text{(Eq 1)}$$

$$T_c(x) = T_C + C_3 e^{m_c x} + C_4 e^{-m_c x} \quad \text{(Eq 2)}$$

$$T_f(x) = T_F + C_5 e^{m_f x} + C_6 e^{-m_f x} \quad \text{(Eq 3)}$$

Here, $C_1$ to $C_6$ are constants that are calculated depending on the boundary conditions of the gripper structure. $T_H$, $T_C$ and $T_F$ are determined by $T_0$ as shown in Eq. 4 for the hot arm, cold arm and flexure, respectively, and $m_h$, $m_c$ and $m_f$ are to be calculated for the gripper components using Eq. 5 (Ref 30).

$$T_0 = T_s + \frac{J^2 \rho}{k_p m^2} \quad \text{(Eq 4)}$$

$$m = \sqrt{\frac{S}{k_p t R_t}} \quad \text{(Eq 5)}$$

Here, $T_s$ is the substrate temperature, $J$ is the current density, $k_p$ is the thermal conductivity of the photoconductive resin, $S$ is known as the shape factor that quantifies the impact of a component's shape on heat conduction to the substrate, $t$ is the thickness of the structure, and $R_t$ is the thermal resistance improved between the suspended gripper and the substrate (Ref 55).

The asymmetric thermal expansion of the hot and cold arms is the driving mechanism behind the electrothermal actuation of the submitted micro-gripper design. Under an applied voltage, the wider arm undergoes less resistive heating and thermal expansion than the narrower arm, resulting in angular rotation of the arms about the fixed anchor pads against the cold arm side. The relative rotation angle for the opening movement of micro-gripper arm is decided by the reverse tangent of the ratio of the arm tip displacement to the total length of the hot arm and the micro-gripper arm (Ref 56). The steady-state lateral displacement at the gripping arm tip, $u_{tip}$, is determined by extrapolating the deviation at the free end of the gripper over the length of the extending micro-gripper arm ($L_a$).

$$u_{tip} = \frac{L_h^2}{6El_h}(X_1 L_h - 3X_2) + \frac{L_a L_h}{2El_h}(X_2 L_h - 2X_3) \quad \text{(Eq 6)}$$

Here, $L_h$ is the length of the hot arm, $E$ is the Young's modulus of resin, $l_h$ is the moment of inertia for the hot arm, and $X_1$, $X_2$ and $X_3$ are the chosen unnecessary loads moving on the gripper. The energy method is applied to analyze the bending moment of the gripper due to these 3 unnecessary loads, which are then computed by solving the following set of simultaneous equation (Eq. 7) (Ref 57).

$$\begin{bmatrix} f_{11} & f_{12} & f_{13} \\ f_{21} & f_{22} & f_{23} \\ f_{31} & f_{32} & f_{33} \end{bmatrix} \begin{bmatrix} X_1 \\ X_2 \\ X_3 \end{bmatrix} = \begin{bmatrix} 0 \\ \Delta L_h - \Delta L_c - \Delta L_f \\ 0 \end{bmatrix} \quad \text{(Eq 7)}$$

Here, the calls $f_{ij}$ symbolize flexibility coefficients that describe the deviation at i owing to a unit load at $j$. $\Delta L_h$, $\Delta L_c$, and $\Delta L_f$ symbolize the total change in length for each of the hot arm, cold arm and flexure components, respectively, and are consisted of the thermal expansion component and the mechanical component that results from the expansion restriction (Ref 57). Moreover, the elements of the mentioned matrix are given as follows:

$$f_{11} = \frac{2s}{EN} + \frac{s^3}{3EI} + \frac{Ss^2}{EI},\ f_{12} = \frac{3S^2 s}{2EI} + \frac{Ss^2}{2EI},\ f_{13} = -\frac{s^2}{2EI} - \frac{Ss}{EI}$$
$$f_{21} = \frac{Ss^2}{2EI} + \frac{3S^2 s}{2EI},\ f_{22} = \frac{s}{EN} + \frac{S^2 s}{EI} + \frac{8S^3}{3EI},\ f_{23} = -\frac{2S^2}{EI} - \frac{Ss}{EI}$$
$$f_{31} = -\frac{s^2}{EI} - \frac{Ss}{EI},\ f_{32} = -\frac{2S^2}{EI} - \frac{Ss}{EI},\ f_{33} = \frac{2S}{EI} + \frac{s}{EI} \quad \text{(Eq 8)}$$

Here, $E$ is Young's modulus of the micro-gripper material resin, and $s$ is the central beam length of the U-beam. Furthermore, $N$ symbolizes the cross section area of the U-beam and $I$ is the moment of inertia.

The lateral displacement acquired at the micro-gripper arm tips is affected among others by the micro-gripper length, the flexure length and the resulting temperature variation between the hot and cold arms. Moreover, in a hot and cold arm design, the hot arm, and the flexure are usually fabricated with the same width dimension, which is generally the smallest feature width that the manufacturing process is able to achieve. Though the flexure has the same width as the hot arm, the temperature improved on the flexure is much lower than that on the hot arm owing to the flexure's shorter length. These opinions of the flexure length and width provide that the micro-gripper is correctly designed to let suitable elastic deviation. The geometrical dimensions of the studied micro-gripper are given in Table 1.

### 2.3 Stereolithography Method

Stereolithography (SLA) is a 3D printer method from the vat photopolymerization family. The most important feature of this method is that it can fabricate fast and with high precision due to its use of high resolution projection. Recently, SLA technology has been preferred in many fields such as micro and nano applications, microfluidic and biomedical (Ref 58, 59).

We show the fabrication process of the SLA method and the internal view of the 3D printer in Fig. 3. This process takes place:

- First, we positioned the building platform in the liquid tank at a layer height for the surface of the liquid.
- After positioning, we reflect the image of the first layer on the building platform and the UV laser beam selectively hardens and solidifies the photopolymer resin to form the layer.
- When the first layer is finished, the platform moves to a safe distance and prepares for the next layer. These processes continue until we completed the complete piece.
- After the complete part is finished, the part fabricated from the 3D printer is taken. We did not fully cure this part and requires UV light finishing if high surface quality, high mechanical and thermal properties are required.

To fabricate the micro-gripper, we used a bottom-up 3D printer system. The Anycubic Photon Mono X 3D printer (company, city, state abbrev if USA, country), which is one of the desktop 3D printers fitted with a 405 nm laser with 30 $\mu$m XY resolution and 10 $\mu$m dynamic Z resolution, was used in this study. The highest printing speed is 50 mm/hour, with a maximum building scale of 192 $\times$ 120 $\times$ 245 mm. The masking method generally consists of three kinds: liquid crystal display (LCD), digital micro mirror device (DMD), and liquid crystal on silicon (LcoS). This printer is manufactured with LCD based SLA printing technology and uses a 4K monochrome LCD as its light source.

### 2.4 Simulation Model

In this section, a finite element analysis (FEA) model has been developed that calculates and analyzes the electrical, thermal and displacement behavior of the micro-gripper designed using the COMSOL Multiphysics program. The analysis of the micro-gripper is divided into two parts: electrothermal and displacement analysis. The electrothermal analysis process consists of converting the dispersion values calculated by the solvent into data points reflecting the Joule heating effects resulting from the current resulting from the application of voltage. In the displacement analysis process, the displacement of the micro-gripper in the lateral plane (y-axis) as a result of the applied voltage was examined. During both the electrothermal and displacement analysis process, voltage

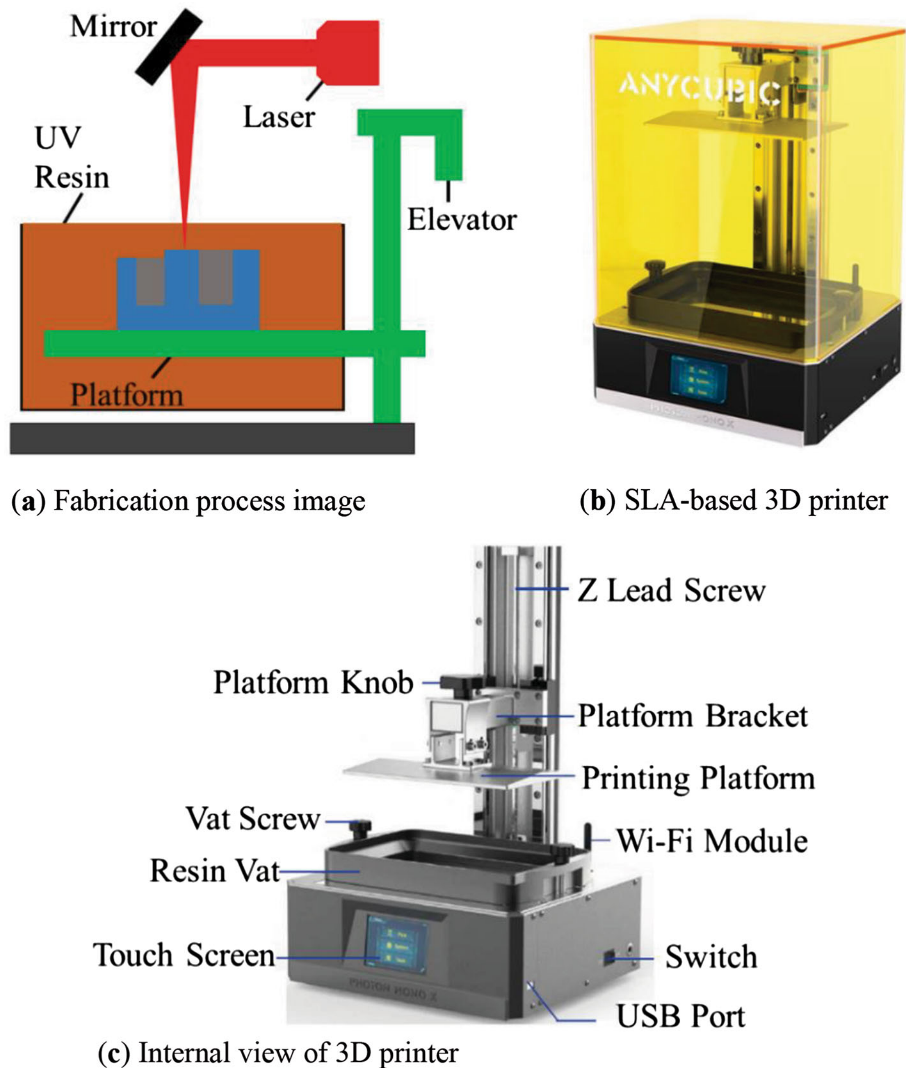


**Fig. 3** Schematic of the SLA method

will be applied to the micro-gripper. During the simulation, a meshing sequence was defined to improve the accuracy of the results and achieve a faster computation time. The maximum and minimum element size for the overall meshing sequence was set to 38.5 and 2.8 $\mu$m, respectively. The maximum element growth rate was set to 1.45, with a curvature factor of 0.4. The computational complexity and size of the model were reduced by using swept meshing method for each component in the overall model. The face meshing method was selected to be quadrilateral. For perovskite layer, the mesh was swept with the number of elements = 40 and element ratio = 0.15.

The model of the micro-gripper created in COMSOL consists of a single layer. During the analysis, the material properties were chosen the same as the photoconductive resin given in Table 2. The model created for simulation requires the application of boundary conditions within the electrical, thermal and mechanical fields. For electrical and mechanical boundary condition, the micro-gripper is fixed from the pads, while the other arms are free to move. In this case, electrical voltage is applied from the pads and the gripper is opened and closed. Thermal boundary conditions consisted of applying a homogeneous room temperature (293K) as an initial condition to all model elements. As the substrate works as a heat sink, it was assumed to be at room temperature along the analysis. Since the probe pads are anchored to the substrate, the bottom surface of the pads was set to the constant substrate temperature (293K). The small dimensions of the micro-gripper allowed the convective heat transfer coefficient of its bottom surface to be modeled by conduction through the air gap to the substrate.

## 3. Fabrication and Experimental Setup

### 3.1 Fabrication of the Micro-Gripper

The fabrication process of the micro-gripper using a 3D printer is shown in Fig. 4. The 3D fabrication process requires a CAD model of the part that can be designed or created from reverse engineering. The 3D CAD model was converted to the STL format to define the finished micro-gripper during the fabrication process. With this format, the micro-gripper is represented by triangular surfaces defined by x, y and z coordinates. Then, the STL file of the micro-gripper was sliced

**Table 2 Properties of resin material**

| Property | Value | Unit |
|---|---|---|
| Density (liquid) | 1.65 | g/(cm$^3$) |
| Density (solid) | 1.65 | g/(cm$^3$) |
| Young's modulus | 375 | MPa |
| Hardness | 120 | MPa |
| Tensile strength | 12 | … |
| Thermal conductivity | 45 | W/m°C |
| Thermal expansion | $6.2 \times 10^{-4}$ | $\mu$m/C |
| Temperature coefficient | $1.75 \times 10^{-5}$ | *ppm*/°C |
| Convective heat transfer coefficient | 4.558 | W/(m$^2$°C) |
| Electrical resistivity | $8.5 \times 10^{-2}$ | Ωμ |
| Glass transition temperature | 350 | °C |
| Service temperature | 320 | °C |
| Relative permittivity | 2.5 | … |

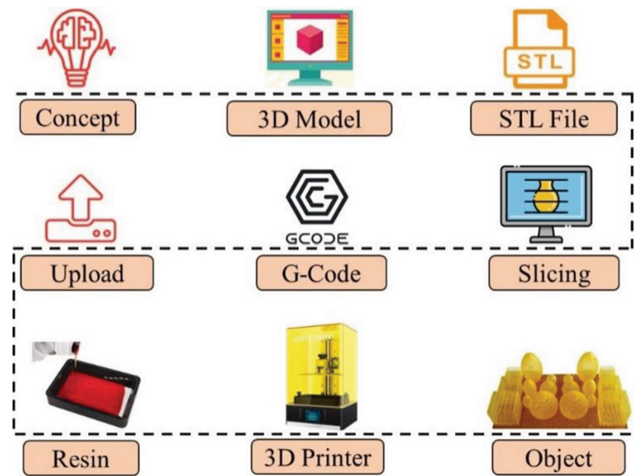


**Fig. 4** The flow chart of the 3D printing process

with the slicing program. This program converts the 3D model into G code language that the printer can understand. The 3D printer is turned on and the G code is transferred to the printer via USB. The parameters of the printer must be entered after the transfer process. To successfully complete the fabrication process, it is necessary to determine the best value for each printing parameter. The parameters for this study were determined by trial and error method. Because the aim is to fabricate the smallest micro-gripper with a 3D printer. For this reason, many grippers have been fabricated by changing the parameters and printing parameters have been determined for optimum fabrication. These parameters are exposure time, curing time, and layer thickness. These parameters are determined as 7s, 6s, and 5 $\mu$m, respectively. After parameter definition, the photoconductive resin is poured into the vat and the 3D printer starts working. The fabrication process with 3D printer continues as described in Sect. 2.3 until all layers of the micro-gripper are fabricated and the process is completed.

In the 3D fabrication process, it is possible to create 3D structures using plastic or polymer-based materials. In this study, photoconductive resin, which is a photopolymer, was used as a material for the SLA method. This resin has a structure that can be photo polymerized. It is also an electrically conductive material. The resin is viscose and designed for 3D printing devices. Because of such features, the use of resin type materials in MEMS has become widespread. Some of the electrical and mechanical properties of the photoconductive resin are given in Table 2.

An image of the micro-gripper fabricated in a 3D printer is shown in Fig. 5. We got some unsuccessful results during fabrication. It was determined that this was because of the insufficient number of supports in the cold, hot, and flexure arms. When the number of supports was low, collapses occurred in the micro-gripper. For this reason, we have achieved fabrication by increasing the number and density of supports over the micro-gripper. The optimum support number for this study was determined to be 16. It listed geometry parameters used during fabrication in Table 1.

### 3.2 Experimental Setup

The micro-gripper fabricated by the fabrication process defined in Sect. 3.1 was mounted on a probe station to make experimental testing and electrical characterization. The exper-

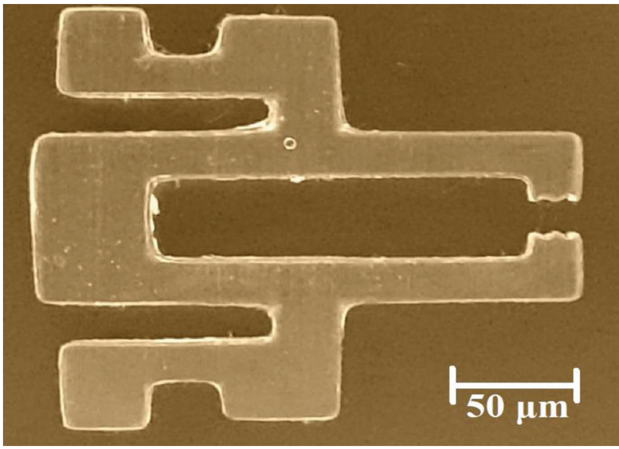


**Fig. 5** The microscope image of the micro-gripper fabricated using SLA-based 3D printer

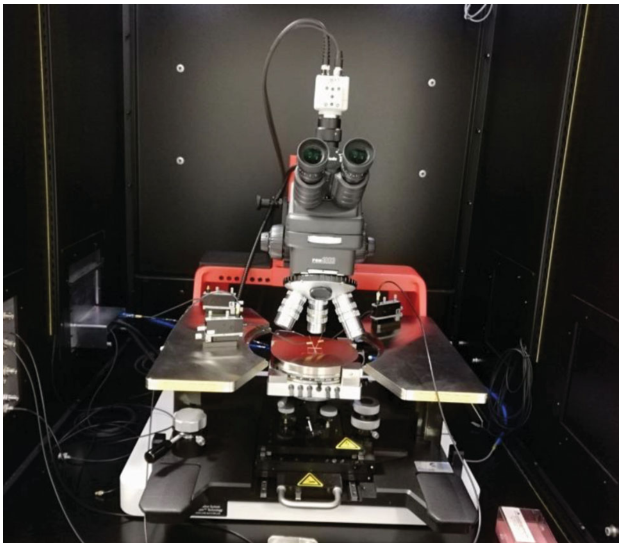

**Fig. 6** The micro-gripper mounted on the platform of the probe station

imental setup is shown in Fig. 6. The experimental setup consists of a probe station, power supply, optical microscope and digital camera. The micro-gripper, which is connected to the station for characterization, is connected with a circuit board with cables connected to electric pads. Then voltage is applied to the micro-gripper using the power supply and voltage probes, each of which has a 3-axis positioning system. An optical microscope and digital camera setup was used to measure the displacement of the micro-gripper as a result of the applied voltage.

The operating voltage for the micro-gripper was determined experimentally. The voltage value was increased in 1V increments until deterioration or breakage of the micro-gripper structure was observed. To check that steady state conditions were reached, the interval between each step was kept more than 10 s.

## 4. Results and Discussion

### *4.1 Thermal Analysis*

One of the most important parameters affecting the displacement performance of the micro-gripper is the maximum temperature reached in the gripper structure under the applied voltage values. The peak temperature of the photoconductive resin based micro-gripper must remain within the material boundaries. The maximum temperature at the applied potential of 5V is 619 K and is located near the middle of the hot arms. The design is limited to this temperature value so that higher temperatures do not damage the micro-gripper structure and pads. Also in healthcare applications, the operating temperature of the micro-gripper plays a critical role due to manipulation of living cells. As a result of the applied voltage value of 5V, it was observed that the temperature at the arm tips of the micro-gripper was close to the room temperature (Fig. 7).

It can be said that the micro-gripper can be used safely in many MEMS areas due to its arm tip temperature reaching around 293K. For the 5V voltage value, the temperature values at the tip, hot, cold and flexure arm of the micro-gripper were calculated 295, 619, 450, and 400K, respectively. It is possible to estimate the arm and maximum temperatures of the micro-gripper with the COMSOL Multiphysics model. For each voltage value, the average temperature values at the tip, hot, cold and flexure arm of the micro-gripper are given in Table 3. As can be understood from the values, as the applied voltage value increased, the maximum temperature increased.

### *4.2 Structural Analysis*

In this section, the simulation, experimental study and maximum stress analysis results of the micro-gripper are examined. With these studies, the opening and closing of the gripper was examined by observing the arm tip displacement. Since the operation of the micro-gripper is electrothermal, when voltage is applied to the pads, the different expansion of the hot and cold arms causes the arm tip of the gripper to move laterally in a curved movement toward the "cold" arm side. Thus, the opening and closing occurs at the tip of the micro-gripper.

The displacement analysis process of the micro-gripper simulation model was performed using finite element analysis. By applying electrical voltage for analysis, the arm tip of the micro-gripper was opened and closed. This operating voltage has been applied from 0V to micro-gripper with 1V increments until breaks or deteriorations are observed in the gripper

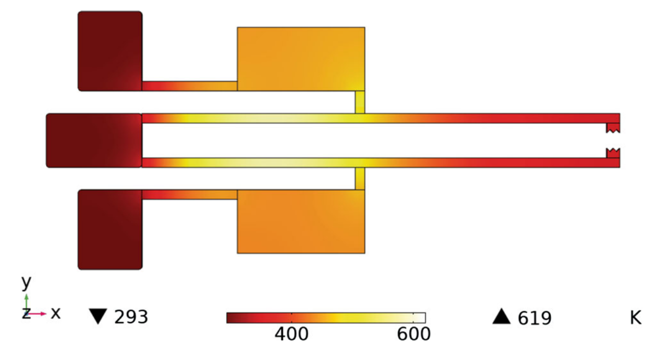


**Fig. 7** Simulated temperature values of the micro-gripper when 5V voltage applied

structure. Positive voltage is applied to the pads on the left and right of the gripper, while the middle pad is grounded (Fig. 1b). The results of simulated lateral displacement of the micro-gripper are shown in Fig. 8.

As can be seen from the results in Fig. 8, the micro-gripper showed lateral displacement without any deterioration in its structure up to 5V voltage value. However, breakages and deteriorations occurred in the arm tip of the micro-gripper after 5V. It has been observed that when 6V voltage is applied to the micro-gripper pads, the gripper moves a maximum of 150.6 $\mu$m. Actually, movement is out of the question here. When Fig. 8 f is examined carefully, it will be seen that there are breaks and distortions in the thin and thick arms. It is seen that analysis on the micro-gripper will not be possible in the case of a 6V voltage application. The voltage values that should be given to the system to characterize the system healthily are revealed by these analyzes. Since the gap opening of the micro-gripper in the closed position is 10 $\mu$m, the lateral displacement values of the micro-gripper in Fig. 8 are calculated as below. For example, at a voltage value of 5V, each arm tip moves 9.97 $\mu$m laterally, and as a result, the total gap opening at 5V is 29.94 $\mu$m.

Electrical characterization was performed using a real-time experimental setup to perform the arm tip displacement analysis of the micro-gripper fabricated. The voltage between 0 and 5V was applied to the micro-gripper connected to the probe station. As a result of electrical voltage, the displacement values at the arm tip of the micro-gripper were determined by the installation

**Table 3 Arm temperature values of the micro-gripper for voltage values**

| Voltage [V] | Hot Arm [K] | Cold Arm [K] | Tip Arm [K] | Flexure Arm [K] |
|---|---|---|---|---|
| 1 | 212 | 125 | 40 | 90 |
| 2 | 356 | 250 | 85 | 150 |
| 3 | 481 | 315 | 125 | 225 |
| 4 | 553 | 385 | 170 | 345 |
| 5 | 619 | 450 | 295 | 400 |

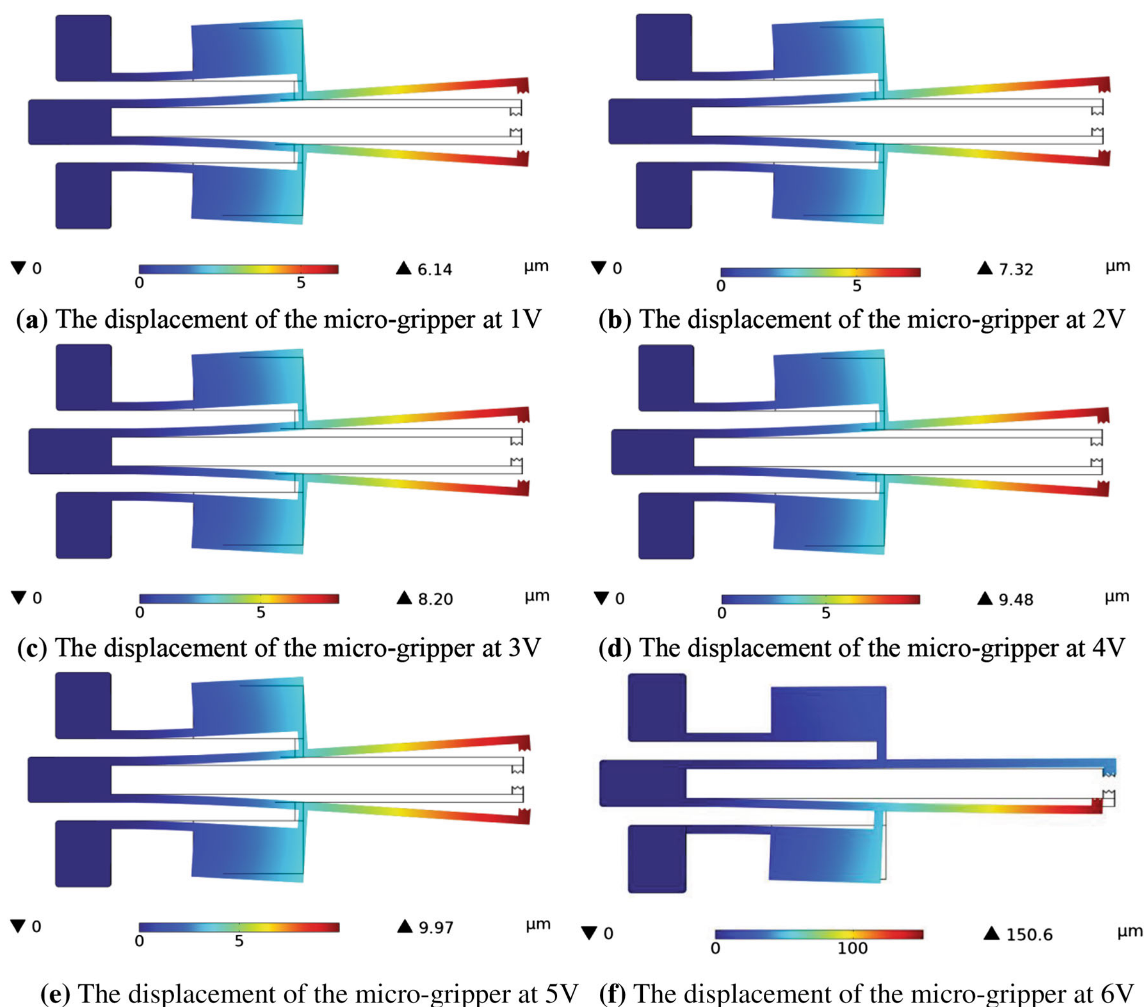


**Fig. 8** Simulated lateral displacement results of all voltages applied to the micro-gripper

of an optical microscope and digital camera. As a result of the characterization, the lateral displacement values of the micro-gripper are shown below. In addition, optical images showing that the fabricated micro-gripper is operated under 5V voltage and when no voltage is applied are given in Fig. 9. The gap opening in the closed position is 10 $\mu$m. A voltage of 5V applied across the micro-gripper arm results in a total gap opening of 28.35 $\mu$m.

In the experimental electrical characterization study, a breakages occurred in the structure of the micro-gripper after 5V voltage value. The displacement values obtained as a result of experimental studies are shown in Fig. 10. According to these values, as the voltage value increases, the displacement of the micro-gripper's arm tip increased. It can be seen that the results of the model obtained as a result of the simulations made with finite element analysis correspond very well with the experimental results (Fig. 10). The displacement error values between simulation and experimental results for 1, 2, 3, 4 and 5V voltage values were measured as 9.80, 9.69, 6.95, 8.95, and 7.45%, respectively.

The minor differences observed between simulation and experimental results for the displacement of the micro-gripper handle tip may be because of many factors, including the electrical, thermal and mechanical properties of the photoconductive resin material. We can also assume that the nonlinear material properties varying with temperature at low voltages are constant because of the low temperatures in the micro-gripper. However, increasing the maximum temperature makes this assumption obsolete, and capturing the nonlinear temperature dependency behavior becomes very important when modeling devices at high operating temperatures.

Another important parameter that affects the performance of the micro-gripper is the resulting stress values. For this reason, it is necessary to investigate the maximum stress that occurs when the micro-gripper is operating, both in terms of size and position. The maximum stresses caused by the application of 5V voltage to the micro-gripper are shown in Fig. 11. The maximum values appeared at the junction of the hot arms with the pads and at the connector, combining the hot and cold arms. At the potential of 5, the maximum Von Mises stress approaches 85 MPa, which is far less than the value of allowable stress. The fracture strength of the photoconductive resin material is 1.8 $\pm$ 0.4 GPa in tensile tests.

Another important factor is the out-of-plane curvatures of oscillating structures due to residual stresses exposed during the fabrication of the micro-gripper. Residual stresses are elastic stresses that remain in the part after various fabrication process and significantly affect the performance and life of the part. Since the micro-gripper is operated electrothermal, the residual stresses can be caused by a thermal mechanical mismatch due to differences in thermal expansion coefficients between different layers of material that are brought together and subjected to a temperature difference, as well as internal stresses arising during the fabrication process. The presence of such residual stress is inherent in the fabrication process and, in the case of a commercially available process used in this work, is beyond the user's control. However, such residual stress distributions can be characterized experimentally and entered as a pre-stress value for the material in the numerical model of the micro-gripper. The application of such considerations is necessary to improve the functionality of the designed micro-gripper and to reduce its failure or failure during deformability characterization. In our next study, the measurement and characterization of residual voltage values on micro-gripper will be performed.

### 4.3 Discussion

We showed a comparison of experimental and finite element analysis results in Fig. 10. When the simulation results are taken as a comparison, it is seen that the maximum displacement errors between the experimental study and the simulation results do not exceed 10%. These differences may be due to established analysis models that only consider bending deformations, while the simulation study takes into account all deformations. It can also depend on many factors, including the electrical, thermal and mechanical properties of the photoconductive resin material. More accurate simulation models will be derived in future studies.

When comparing existing micro-grippers, the superiority of this fabrication is obvious. Because while MEMS type grippers in the literature were fabricated with conventional fabrication techniques, additive manufacturing technique was used in this study. As suggested in the literature, micro-grippers provide

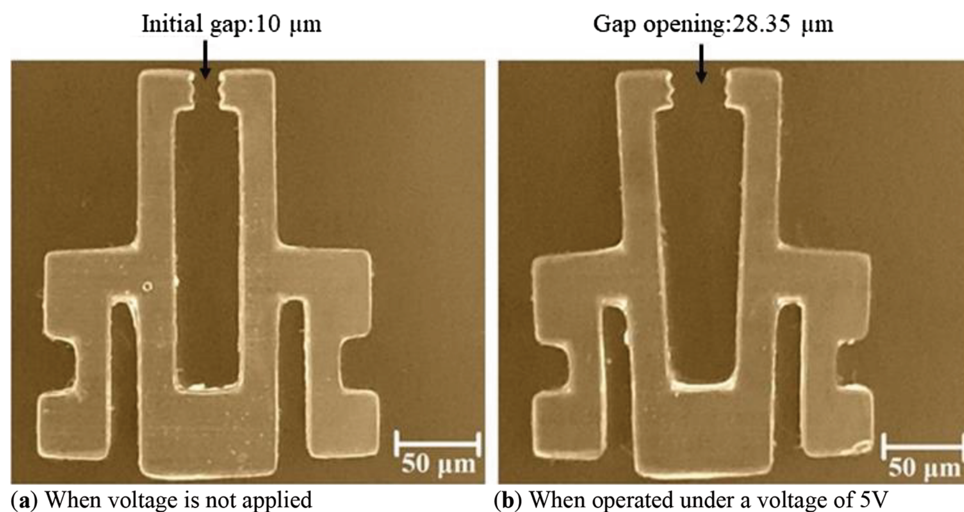


(**a**) When voltage is not applied (**b**) When operated under a voltage of 5V

**Fig. 9** Optical images of the micro-gripper fabricated

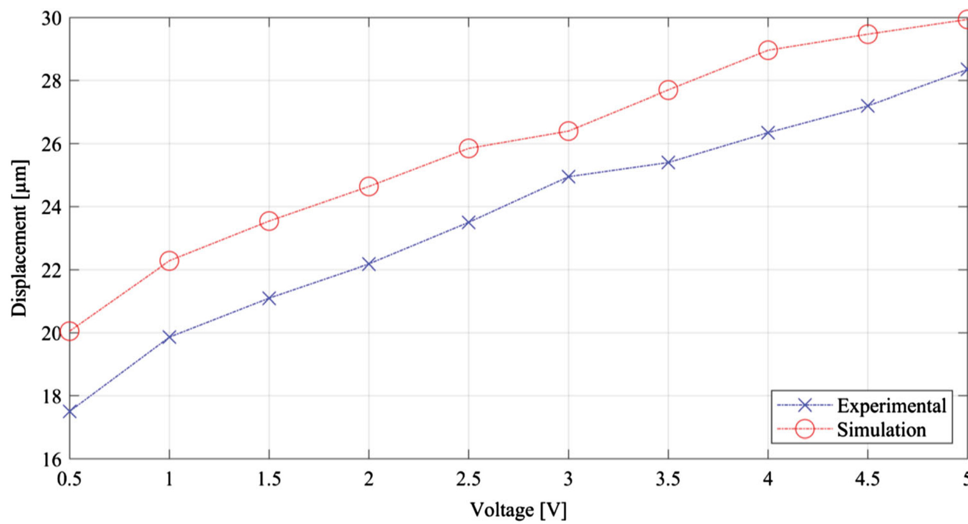


**Fig. 10** Simulated and experimental lateral displacement values of the micro-gripper

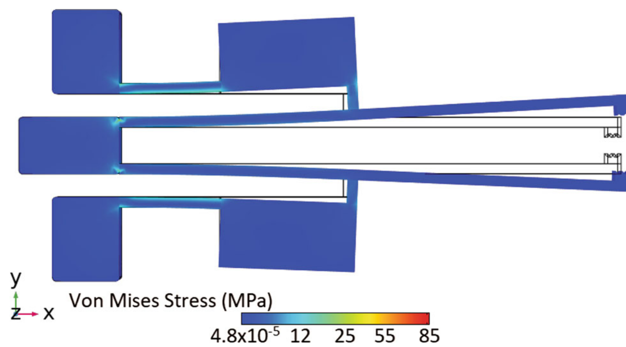


**Fig. 11** Von Mises stresses occurred at a potential of 5 V within the micro-gripper structure

displacements of 25 $\mu$m (Ref 52), 80 $\mu$m (Ref 53), 60 $\mu$m (Ref 60), and 63 $\mu$m (Ref 61) from high input voltages of 5, 6, 70, and 72V, respectively. In this article, a tip displacement of 28.35 $\mu$m was easily achieved with a low operation voltage of 5V, contributed by the apparent capacity of the U-type electrothermal actuator used in conjunction with a new structure design. However, after the voltage value of 5V, breaks and distortions occurred at the tip arm of the micro-gripper. By changing the size of the designed micro-gripper, fabrications resistant to higher voltages can be made. Thus, higher tip displacements can be achieved.

There are also some MEMS grippers operated by thermal actuators in previous work. For example, a micro-gripper actuator with integrated V-beam thermal capability has been reported in the literature (Ref 62). This actuator generates a force in the y-axis direction, and the force is transmitted from the y-axis to the x-axis direction using a displacement amplification bend. While this bending causes a relatively large loss of displacement in the vertical direction, it is not as accurate when performing a clutch operation. In addition, an electro thermally actuated arrester can be found in the literature (Ref 63). This gripper has a simple working principle. However, the complex mechanical structure complicates the manufacturing process. By comparison, the U-type electrothermal micro-gripper presented in this article has advantages such as easy fabrication and less impact of manufacturing defects on the functionality of the gripper.

## 5. Conclusions

A new electrothermal MEMS micro-gripper has been designed, simulated, fabricated, and experimentally tested in this paper. Electrothermal actuation is used in the displacement of the gripper and it is designed to be suitable for use in many areas by providing a very low temperature at the arm tips of the micro-gripper during actuation. The fabrication of the micro-gripper was done using a SLA based 3D printer with a resolution of 30 $\mu$m. The most successful fabrication was carried out in the dimensions of the micro-gripper 1050 $\mu$m long, 285 $\mu$m wide and 5 $\mu$m thick.

An electrical characterization setup was created for the experimental study. Electrical voltage was applied to the micro-gripper placed in the station, starting from 1 to 1V increments, until deterioration or breakage was observed in the gripper structure. It has been determined that the micro-gripper can with-stand a maximum voltage of 5V. As a result of the characterization, each micro-gripper arm had a maximum in-plane displacement of around 9 $\mu$m at 5V, resulting in a total micro-gripper opening of 28.35 $\mu$m. The simulation and experimental results for the displacement of the micro-gripper arm tips are all in good agreement. The displacement error values between simulation and experimental results for 1, 2, 3, 4, and 5V voltage values were measured as 9.80, 9.69, 6.95, 8.95, and 7.45%, respectively.

In our next study, the micro-gripper whose voltage and displacement performance is observed will be developed to include force feedback. Grip force measurements will be provided by the integration of capacitive force sensors into the design. These measurements are important for the micro-gripper to grasp the objects precisely and without damaging them. Object gripping and release will be achieved by applying the operating voltage and the resulting gripping force will be determined as feedback.

## References


1. R.R. Syms and S. Wright, MEMS Mass Spectrometers: The Next Wave of Miniaturization, *J. Micromech. Microeng.*, 2016, **26**, p 023001.
2. J. Iannacci, Reliability of MEMS: A Perspective on Failure Mechanisms, Improvement Solutions and Best Practices at Development Level, *Displays*, 2015, **37**, p 62–71. https://doi.org/10.1016/j.displa.2014.08.003
3. J. Chai, K. Zhang, Y. Xue, W. Liu, T. Chen, Y. Lu and G. Zhao, Review of MEMS Based Fourier Transform Spectrometers, *Micromachines*, 2020, **11**, p 214. https://doi.org/10.3390/mi11020214
4. S. Yang and Q. Xu, A Review on Actuation and Sensing Techniques for MEMS-Based Microgrippers, *J. Micro-Bio Robot.*, 2017, **13**, p 1–14. https://doi.org/10.1007/s12213-017-0098-2
5. Vurchio, F., Orsini, F., Scorza, A., Sciuto, S.A. Functional Characterization of MEMS Microgripper Prototype for Biomedical Application: Preliminary Results. In Proceedings of the 2019 IEEE International Symposium on Medical Measurements and Applications (MeMeA), Istanbul, Turkey, IEEE, 26–28 (2019), pp. 1–6, doi: https://doi.org/10.1109/MeMeA.2019.8802178
6. Bagolini, A., Bellutti, P., Di Giamberardino, P., Rudas, I.J., D'Andrea, V., Verotti, M., Dochshanov, A., Belfiore, N.P. Stiffness Characterization of Biological Tissues by Means of Mems-Technology Based Micro Grippers Under Position Control. In International Conference on Robotics in Alpe-Adria Danube Region, (Springer, Cham, Switzerland, 2017), pp. 939–947
7. Leester-Schaedel, M., Gursky, B., Garces-Schroeder, M., Vierheller, A., Matheis, B., Buetefisch, S., Rustenbeck, I., Boel, M., Dietzel, A. Micro-Grippers for Biomedical and Biomechanical Studies. In Proceedings of the ACTUATOR 2018; 16th International Conference on New Actuators, (Bremen, Germany, 25–27 2018) VDE: 2018, pp. 1–4
8. M. Maroufi, H. Alemansour, M.B. Coskun and S.O.R. Moheimani, An Adjustable-Stiffness MEMS Force Sensor: Design, Characterization, and Control, *Mechatronics*, 2018, **56**, p 198–210. https://doi.org/10.1016/j.mechatronics.2018.05.007
9. P. Wang, Y. Liu, D. Wang, H. Liu, W. Liu and H. Xie, Stability Study of an Electrothermally-Actuated MEMS Mirror with Al/SiO2 Bimorphs, *Micromachines*, 2019, **10**, p 693. https://doi.org/10.3390/mi10100693
10. O. Ulkir, Design and Fabrication of an Electrothermal MEMS Micro-Actuator with 3D Printing Technology, *Mater. Res. Express*, 2020, **7**, 075015. https://doi.org/10.1088/2053-1591/aba8e3
11. C. Sano, M. Ataka, G. Hashiguchi and H. Toshiyoshi, An Electret-Augmented Low-Voltage MEMS Electrostatic Out-of-Plane Actuator for Acoustic Transducer Applications, *Micromachines*, 2020, **11**, p 267. https://doi.org/10.3390/mi11030267
12. van Spengen, W. M. The electrostatic actuation of MEMS with high voltage amplifiers From comb drive levitation and pull-in to dielectric charging and position noise
13. Garcés-Schröder, M., Hecht, L., Vierheller, A., Leester-Schädel, M., Böl, M., Dietzel, A. Micro-Grippers with Femtosecond-Laser Machined In-Plane Agonist-Antagonist SMA Actuators Integrated on Wafer-Level by Galvanic Riveting. Proceedings 2017, 1, 385, doi:https://doi.org/10.3390/proceedings1040385
14. V.R.C. Kode and M.C. Cavusoglu, Design and Characterization of a Novel Hybrid Actuator Using Shape Memory Alloy and Dc Micromotor for Minimally Invasive Surgery Applications, *IEEE/ASME Trans. Mechatron.*, 2007, **12**(4), p 455–464.
15. K.S. Rao, M. Hamza, P.A. Kumar and K.G. Sravani, Design and Optimization of Mems Based Piezoelectric Actuator for Drug Delivery Systems, *Microsyst. Technol.*, 2019, **26**, p 1671–1679. https://doi.org/10.1007/s00542-019-04712-9
16. S. Tuncdemir, S.O. Ural and K. Uchino, Meso-Scale Piezoelectric Gripper with High Dexterity, *Japan. J. Appl. Phys.*, 2009, **48**(4R), p 044501.
17. J. Yunas, B. Mulyanti, I. Hamidah, M.M. Said, R.E. Pawinanto, W.A.F.W. Ali, A. Subandi, A.A. Hamzah, R. Latif and B.Y. Majlis, Polymer-Based MEMS Electromagnetic Actuator for Biomedical Application: A Review, *Polymers*, 2020, **12**, p 1184. https://doi.org/10.3390/polym12051184
18. S. Yang and Q. Xu, A review on Actuation and Sensing Techniques for MEMS-Based Microgrippers, *Journal of Micro-Bio Robotics*, 2017, **13**(1), p 1–14.
19. Y. Wu, T. Jiang, Q. Lu, C. Xia, J. Fu, Y. Wang and Z. Wu, Characteristics of Thermally Actuated Pneumatic Proportional Pressure Valves and Their Application, *J. Inst. Eng. Ser. C*, 2020, **101**, p 631–641. https://doi.org/10.1007/s40032-020-00574-7
20. Bouhadda, I., Mohand-Ousaid, A., Le Moal, P., Bourbon, G., Lutz, P. Dynamic Characterization of an Electrothermal Actuator Devoted to Discrete MEMS Positioning. In Proceedings of the 2017 Symposium on Design, Test, Integration and Packaging of MEMS/MOEMS (DTIP), (Bordeaux, France, 29 May–1 2017), IEEE, 2017, pp. 1–4
21. M. Lara-Castro, A. Herrera-Amaya, M.A. Escarola-Rosas, M. Vázquez-Toledo, F. López-Huerta, L.A. Aguilera-Cortés and A.L. Herrera-May, Design and Modeling of Polysilicon Electrothermal Actuators for a MEMS Mirror with Low Power Consumption, *Micromachines*, 2017, **8**, p 203. https://doi.org/10.3390/mi8070203
22. S. Iqbal and A. Malik, A Review on MEMS based Micro Displacement Amplification Mechanisms, *Sens. Actuators A Phys.*, 2019, **300**, 111666. https://doi.org/10.1016/j.sna.2019.111666
23. Ruggeri, S., Fontana, G., Legnani, G., Fassi, I. Design Strategies for Vacuum Micro-Grippers with Inte-Grated Release System. In International Design Engineering Technical Conferences and Computers and Information in Engineering Conference, American Society of Mechanical Engineers, Ohio, (USA, 6-9 2017), 2017, pp. 1-7
24. K. Alblalaihid, J. Overton, S. Lawes and P. Kinnell, A 3D-Printed Polymer Micro-Gripper with Self-Defined Electrical Tracks and Thermal Actuator, *J. Micromech. Microeng*, 2017, **27**, p 1–10. https://doi.org/10.1088/1361-6439/aa6de8
25. R.S. Joshi, A.C. Mitra and S.R. Kandharkar, Design and Analysis of Compliant Micro-gripper Using Pseudo Rigid Body Model(PRBM), *Mater. Today Proc.*, 2017, **4**, p 1701–1707. https://doi.org/10.1016/j.matpr.2017.02.010
26. Pham, P. H., & Bui, D. V. Single Mask and Low Voltage of Micro Gripper Driven by Electrothermal V–Shaped Actuator. In IFToMM Asian Conference on Mechanism and Machine Science. (Springer, Cham, 2021), pp. 693-704
27. Nguyen, D. C., Phan, T. V., & Pham, H. T. Design and analysis of a compliant gripper integrated with constant-force and static balanced mechanism for micro manipulation. In 2018 4th International Conference on Green Technology and Sustainable Development (GTSD), IEEE 2018, pp. 291-295
28. Wu, Z., & Chen, M. Model and Study of Clamping Force for Micro-gripper with PZT-driven. In 2019 WRC Symposium on Advanced Robotics and Automation (WRC SARA) IEEE 2019, pp. 74-79
29. M. Verotti, A. Dochshanov and N.P. Belfiore, A Comprehensive Survey on Microgrippers Design: Mechanical Structure, *Journal of Mechanical Design*, 2017, **139**(6), p 060801.
30. M. Cauchi, I. Grech, B. Mallia, P. Mollicone and N. Sammut, Analytical, Numerical and Experimental Study of a Horizontal Electrothermal MEMS Microgripper for the Deformability Characterisation of Human Red Blood Cells, *Micromachines*, 2018, **9**(3), p 108.
31. A. Dochshanov, M. Verotti and N.P. Belfiore, A Comprehensive Survey on Microgrippers Design: Operational Strategy, *J. Mech. Design*, 2017, **139**(7), p 070801.
32. A. Bagolini, S. Ronchin, P. Bellutti, M. Chistè, M. Verotti and N.P. Belfiore, Fabrication of Novel MEMS mi-crogrippers by Deep Reactive Ion Etching with Metal Hard Mask, *J. Microelectromech. Syst.*, 2017, **26**, p 926–934. https://doi.org/10.1109/JMEMS.2017.2696033
33. N. Chronis and L.P. Lee, Electrothermally Activated SU-8 microgripper for Single Cell Manipulation in Solution, *J. Microelectromech. Syst.*, 2005, **14**(4), p 857–863.
34. Y.-Y. Feng, S.-J. Chen, P.-H. Hsieh and W.-T. Chu, Fabrication of an Electro-Thermal Micro-Gripper with Elliptical Cross-Sections using Silver-Nickel Composite Ink, *Sens. Actuators A Phys.*, 2016, **245**, p 106–112. https://doi.org/10.1016/j.sna.2016.04.045
35. C. Potrich, L. Lunelli, A. Bagolini, P. Bellutti, C. Pederzolli, M. Verotti and N.P. Belfiore, Innovative Silicon Microgrippers for Biomedical Applications: Design, Mechanical Simulation and Evaluation of Protein Fouling, *In Actuators*, 2018, **7**, p 12. https://doi.org/10.3390/act7020012
36. P. Ahangar, M.E. Cooke, M.H. Weber and D.H. Rosenzweig, Current Biomedical Applications of 3D Printing and Additive Manufacturing, *Appl. Sci.*, 2019, **9**, p 1713. https://doi.org/10.3390/app9081713

37. E.B. Joyee and Y. Pan, Additive Manufacturing of Multi-Material Soft Robot for on-Demand Drug Delivery Applications, *J. Manuf. Process.*, 2020, **56**, p 1178–1184.
38. J. Zhang, L. Wei, X. Meng, F. Yu, N. Yang and S. Liu, Digital Light Processing-Stereolithography Three-Dimensional Printing of yttria-Stabilized zirconia, *Ceram. Int.*, 2020, **46**, p 8745–8753. https://doi.org/10.1016/j.ceramint.2019.12.113
39. I. Ertugrul, The Fabrication of Micro Beam from Photopolymer by Digital Light Processing 3D Printing Technology, *Micromachines*, 2020, **11**, p 518. https://doi.org/10.3390/mi11050518
40. P. Feng, P. Wu, C. Gao, Y. Yang, W. Guo, W. Yang and C. Shuai, A Multimaterial Scaffold with Tunable Properties: Toward Bone Tissue Repair, *Advanced science*, 2018, **5**(6), p 1700817.
41. C. Shuai, W. Yang, P. Feng, S. Peng and H. Pan, Accelerated Degradation of HAP/PLLA Bone Scaffold by PGA Blending Facilitates Bioactivity and Osteoconductivity, *Bioactive Materials*, 2021, **6**(2), p 490–502.
42. P. Feng, J. Jia, S. Peng, W. Yang, S. Bin and C. Shuai, Graphene Oxide-Driven Interfacial Coupling in Laser 3D Printed PEEK/PVA Scaffolds For Bone Regeneration, *Virtual and Physical Prototyping*, 2020, **15**(2), p 211–226.
43. P. Feng, Y. Kong, L. Yu, Y. Li, C. Gao, S. Peng and C. Shuai, Molybdenum Disulfide Nanosheets Embedded With Nanodiamond Particles: Co-Dispersion Nanostructures as Reinforcements for Polymer Scaffolds, *Appl. Mater. Today*, 2019, **17**, p 216–226.
44. M. Heidari-Rarani, M. Rafiee-Afarani and A.M. Zahedi, Mechanical Characterization of FDM 3D Printing of Con-Tinuous Carbon Fiber Reinforced PLA Composites, *Compos. Part B Eng.*, 2019, **175**, 107147. https://doi.org/10.1016/j.compositesb.2019.107147
45. P. Robles-Martinez, X. Xu, S.J. Trenfield, A. Awad, A. Goyanes, R. Telford, A.W. Basit and S. Gaisford, 3D Printing of a Multi-Layered Polypill Containing Six Drugs Using a Novel Stereolithographic Method, *Pharmaceutics*, 2019, **11**, p 274. https://doi.org/10.3390/pharmaceutics11060274
46. R. Xiao, M. Ding, Y. Wang, L. Gao, R. Fan and Y. Lu, Stereolithography (SLA) 3D Printing of Carbon fi-ber-graphene oxide (CF-GO) Reinforced Polymer Lattices, *Nanotechnology*, 2021, **32**, 235702. https://doi.org/10.1088/1361-6528/abe825
47. Bahr, R., He, X., Tehrani, B., Tentzeris, M.M. A Fully 3D Printed Multi-Chip Module with an on-Package Enhanced Dielectric Lens for mm-Wave Applications using Multimaterial Stereo-Lithography. In Proceedings of the 2018 IEEE/MTT-S International Microwave Symposium-IMS, Philadelphia, (PA, USA, 10–15 2018) IEEE, 2018, pp. 1561–1564
48. M.G.A. Mohamed, H. Kumar, Z. Wang, N. Martin, B. Mills and K. Kim, Rapid and Inexpensive Fabrication of Multi-Depth Microfluidic Device using High-Resolution LCD Stereolithographic 3D Printing, *J. Manuf. Mater. Process.*, 2019, **3**, p 26. https://doi.org/10.3390/jmmp3010026
49. S.S. Ray, H. Dommati, J.-C. Wang and S.-S. Chen, Solvent based Slurry Stereolithography 3D Printed Hydrophilic Ceramic Membrane for Ultrafiltration Application, *Ceram. Int.*, 2020, **46**, p 12480–12488. https://doi.org/10.1016/j.ceramint.2020.02.010
50. S. Yang and Q. Xu, Design of a Microelectromechanical Systems Microgripper with Integrated Electrothermal Actu-Ator and Force Sensor, *Int. J. Adv. Robot. Syst.*, 2016, **13**, p 1–10. https://doi.org/10.1177/1729881416663375
51. H. Mehrabi, M. Hamedi and I. Aminzahed, A Novel Design and Fabrication of a Micro-Gripper for Manipulation Of Micro-Scale Parts Actuated by a bending piezoelectric, *Microsyst. Technol.*, 2019, **26**, p 1563–1571. https://doi.org/10.1007/s00542-019-04696-6
52. O. Millet, P. Bernardoni, S. Régnier, P. Bidaud, E. Tsitsiris, D. Collard and L. Buchaillot, Electrostatic Actuated Micro Gripper Using an Amplification Mechanism, *Sens. Actuators, A*, 2004, **114**(2–3), p 371–378.
53. R.K. Jain, S. Majumder, B. Ghosh and S. Saha, Design and Manufacturing of Mobile Micro Manipulation System with a Compliant Piezoelectric Actuator Based Micro Gripper, *J. Manuf. Syst.*, 2015, **35**, p 76–91.
54. A.M. El-Sayed, A. Abo-Ismail, M.T. El-Melegy, N.A. Hamzaid and N.A.A. Osman, Development of a Micro-Gripper using Piezoelectric Bimorphs, *Sensors*, 2013, **13**(5), p 5826–5840.
55. L. Lin and M. Chiao, Electrothermal Responses of Lineshape Microstructures, *Sens. Actuators, A*, 1996, **55**(1), p 35–41.
56. Y. Jia and Q. Xu, MEMS Microgripper Actuators and Sensors: The State-of-the-Art Survey, *Recent Patents on Mechanical Engineering*, 2013, **6**(2), p 132–142.
57. Kennedy, J. B., & Murty, M. K. (1990). Elastic Analysis of Structures: Classical and Matrix Methods. Harpercollins College Division
58. P. Juskova, A. Ollitrault, M. Serra, J.-L. Viovy and L. Malaquin, Resolution Improvement of 3D Stereo-Lithography through the Direct Laser Trajectory Programming: Application to Microfluidic Deterministic Lateral Displacement Device, *Anal. Chim. Acta*, 2018, **1000**, p 239–247. https://doi.org/10.1016/j.aca.2017.11.062
59. B.J. Green, K.S. Worthington, J.R. Thompson, S.J. Bunn, M. Rethwisch, E.E. Kaalberg, C. Jiao, L.A. Wiley, R.F. Mullins, E.M. Stone et al., Effect of Molecular Weight and Functionality on Acrylated Poly for Stereolithography and Biomedical Applications, *Biomacromol*, 2018, **19**, p 3682–3692. https://doi.org/10.1021/acs.biomac.8b00784
60. Q. Xu, Design, Fabrication, and Testing of an Mems Microgripper with Dual-Axis Force Sensor, *IEEE Sens. J.*, 2015, **15**(10), p 6017–6026.
61. J. Zhang, J. Gan, H. Ding and H. Li, Design of a Pure Rotation Micropositioning Stage with Dual-Range, *Mechanism and Machine Theory*, 2022, **169**, p 104631.
62. Ali, N., Shakoor, R. I., & Hassan, M. M. (2011). Design, Modeling and Simulation of Electrothermally Actuated Microgripper with Integrated Capacitive Contact Sensor. In 2011 IEEE 14th International Multitopic Conference, IEEE, pp. 201-206
63. B. Hoxhold and S. Büttgenbach, Easily Manageable, Electrothermally Actuated Silicon Micro Gripper, *Microsyst. Technol.*, 2010, **16**(8–9), p 1609–1617.


**Publisher's Note** Springer Nature remains neutral with regard to jurisdictional claims in published maps and institutional affiliations.